Inorganic Chemistry

Article

pubs.acs.org/IC

Uncommon *cis* Configuration of a Metal–Metal Bridging Noninnocent Nindigo Ligand

Prasenjit Mondal,[†] Sebastian Plebst,[‡] Ritwika Ray,[†] Shaikh M. Mobin,[§] Wolfgang Kaim,*[,‡] and Goutam Kumar Lahiri*[,†]

[†]Department of Chemistry, Indian Institute of Technology Bombay, Powai, Mumbai 400076, India

[‡]Institut für Anorganische Chemie, Universität Stuttgart, Pfaffenwaldring 55, D-70550 Stuttgart, Germany

[§]Discipline of Chemistry, School of Basic Sciences, Indian Institute of Technology Indore, Indore 452017, India

Supporting Information

ABSTRACT: In contrast to several reported coordination compounds of *trans*-Nindigo ligands [Nindigo = indigo-bis(*N*-arylimine) = LH_2] with one or two six-membered chelate rings involving one indole N and one extracyclic N for metal binding, the new diruthenium complex ion $[(acac)_2Ru(\mu,\eta^2{:}\eta^2\text{-}L)Ru(bpy)_2]^{2+}$ = $\mathbf{2}^{2+}$ exhibits edge-sharing five- and seven-membered chelate rings in the first documented case of asymmetric bridging by a Nindigo ligand in the *cis* configuration [L^{2-} = indigo-bis(*N*-phenylimine)dianion]. The dication in compound $[\mathbf{2}](ClO_4)_2$ displays one Ru(α-diimine)$_3$ site and one ruthenium center with three negatively charged chelate ligands. Compound $[\mathbf{2}](ClO_4)_2$ is obtained from the $[Ru(bpy)_2]^{2+}$-containing *cis* precursor $[(LH)Ru(bpy)_2]ClO_4$ = $[\mathbf{1}]ClO_4$, which exhibits intramolecular H-bonding in the cation. Four accessible oxidation states each were characterized for the $\mathbf{1}^n$ and $\mathbf{2}^n$ redox series with respect to metal- or ligand-centered electron transfer, based on X-ray structures, electron paramagnetic resonance, and ultraviolet–visible–near-infrared spectroelectrochemistry in conjunction with density functional theory calculation results. The structural asymmetry in the Ru^{III}/Ru^{II} system $\mathbf{2}^{2+}$ is reflected by the electronic asymmetry (class I mixed-valence situation), leaving the noninnocent Nindigo bridge as the main redox-active site.

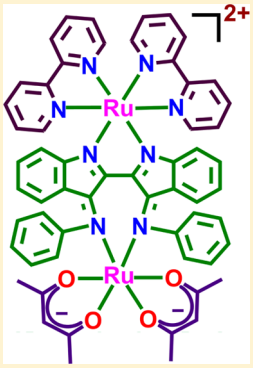

INTRODUCTION

Among the noninnocently behaving ligands,[1] the metal–metal bridging systems attract special attention because of the alternative between the noninnocence of the radical-forming bridge, associated with a homovalent dimetal situation (**A**), and mixed-valence metals (**B**), coupled by an apparently redox-inactive bridge (eq 1).[1,2]

$$\underset{\mathbf{A}}{L_nM^x\text{–}(\mu\text{-}BL^{\bullet-})\text{–}M^xL_n} \text{ vs } \underset{\mathbf{B}}{L_nM^{x+1}\text{–}(\mu\text{-}BL^{2-})\text{–}M^xL_n} \quad (1)$$

Compounds of ruthenium in particular have been studied with respect to options for **A** or **B** (eq 1) in several cases.[2−4]

A more recent addition to the panoply of redox-active ligands has involved the Nindigo = indigo-bis(*N*-arylimine) systems that are derived from the indigo chromophore and can form four different oxidation states following stepwise reduction and deprotonation.[4−9] Nindigo ligands were shown to form homodinuclear complexes with molecular fragments containing B,[6] Pd,[5,7] Co,[8,9] and Ru.[4] Mixed (B/Pd) systems were also reported;[7] all these examples exhibit the original *trans* configuration of the Nindigo chromophore (Scheme 1). One example of a mononuclear palladium(II) complex has been reported in the *cis* configuration and was attributed to space-demanding aryl substituents on the external nitrogen atoms.[5] Instead of the usual β-diketiminato coordination with a six-membered chelate ring, the Pd^{II} center was found as part of a five-membered ring, while the external nitrogen atoms were connected by an intramolecular hydrogen bridge.[5] While boron(III)[6,7] and palladium(II)[5,7] are not expected to undergo one-electron transfers easily in conjunction with redox-active ligands such as Nindigo, it has been shown that the Co and Ru compounds involve redox-active metals.[4,8,9]

One of the most widely employed[2a,3,10,11] ruthenium complex fragments is $[Ru(bpy)_2]^{n+}$, which we have now tried to combine with the Nindigo ligand indigo-bis(*N*-phenylimine). In the course of these investigations, we obtained the first example of *cis*-configured Nindigo as an asymmetrically bis-chelating and redox-active bridge.

Scheme 1 illustrates the configurational isomerism of Nindigo molecules and their deprotonation. Scheme 1 also depicts the chelate coordination alternatives **C** (two six-membered chelate rings) and **D** (one five-membered and one seven-membered chelate ring) for dinuclear complexes.

RESULTS AND DISCUSSION

The mononuclear ruthenium-bis-bipyridine complex ion $[(LH)Ru(bpy)_2]^+$ ($\mathbf{1}^+$) containing the monodeprotonated Nindigo ligand was prepared from *in situ*-generated $[Ru(bpy)_2(EtOH)_2]^{2+}$ and LH_2 = Nindigo = indigo-bis(*N*-phenylimine) in refluxing ethanol in the presence of NEt_3 as a base. The asymmetric dinuclear complex ion $[(acac)_2Ru(\mu,\eta^2{:}\eta^2\text{-}L)Ru(bpy)_2]^{2+}$ ($\mathbf{2}^{2+}$) was obtained by the reaction of precursor $\mathbf{1}^+$ with

Received: June 19, 2014
Published: August 19, 2014

   dx.doi.org/10.1021/ic501460d | *Inorg. Chem.* 2014, 53, 9348−9356

Scheme 1. Alternatives for Bis-chelate Coordination by Deprotonated Nindigo in the *trans* or *cis* Configuration

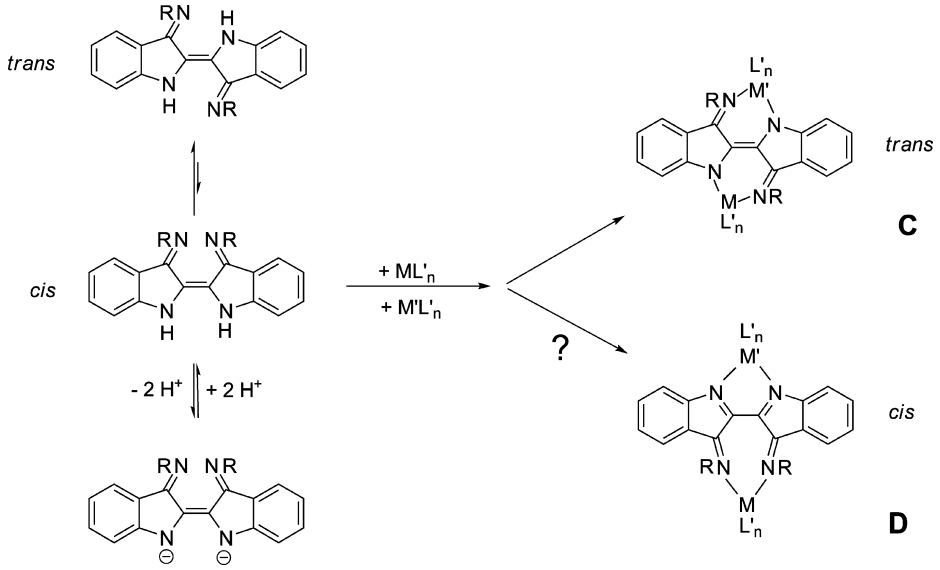

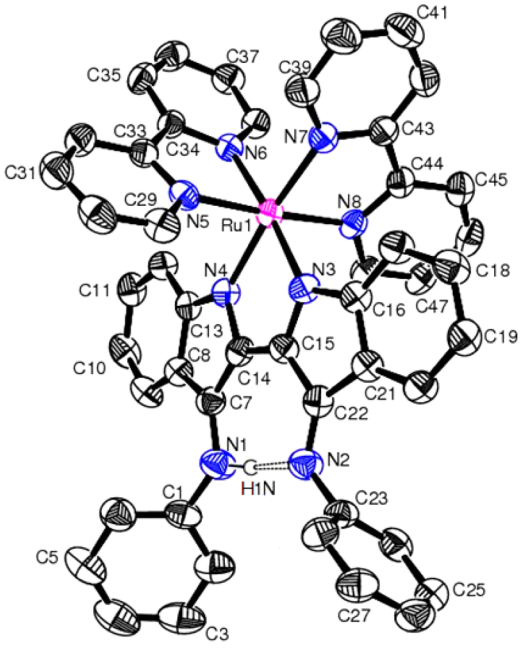

Figure 1. ORTEP diagram of the cationic part of $[\mathbf{1}]ClO_4 \cdot C_7H_8$. Ellipsoids are drawn at the 50% probability level. Hydrogen atoms (except the hydrogen involved in NH···N bonding) and solvent molecules have been omitted for the sake of clarity.

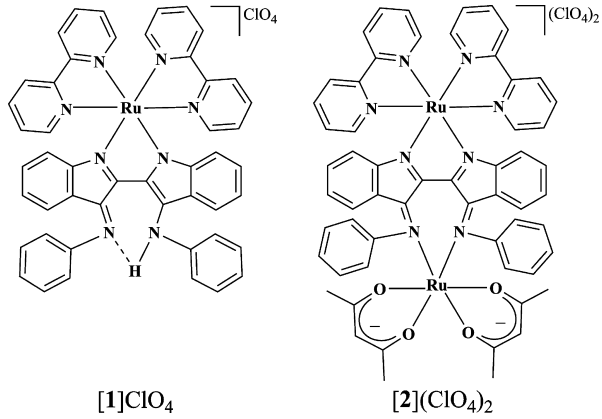

$[Ru(acac)_2(CH_3CN)_2]$ ($acac^-$ = acetylacetonate = 2,5-pentanedionate) in refluxing ethanol. The complexes were purified as perchlorates by column chromatography, using a neutral alumina column (see the Experimental Section). Attempts to prepare the analogous Nindigo-bridged diruthenium–bipyridine complex $[(bpy)_2Ru(\mu\text{-}L)Ru(bpy)_2]^{n+}$ via the direct reaction of 2 equiv of $[Ru(bpy)_2(EtOH)_2]^{2+}$ or $Ru(bpy)_2Cl_2$ with LH_2 or by reacting isolated mononuclear $\mathbf{1}^+$ with another molecule of $[Ru(bpy)_2(EtOH)_2]^{2+}$ or $Ru(bpy)_2Cl_2$ failed.

The 1:1 and 1:2 conducting compounds $[\mathbf{1}]ClO_4$ and $[\mathbf{2}](ClO_4)_2$, respectively, gave satisfactory microanalytical and mass spectral data (Experimental Section and Figure S1 of the Supporting Information). ^{1}H NMR spectroscopy of $[\mathbf{1}]ClO_4$ in $(CD_3)_2SO$ yields 34 partially overlapping proton resonances in the region of 5.0–9.0 ppm (18 and 16 protons of coordinated LH^- and bpy, respectively), in addition to one NH(LH^-) proton signal at 11.5 ppm, corresponding to the full molecule (Figure S2a of the Supporting Information and the Experimental Section). ^{1}H NMR spectroscopy of dinuclear complex $[\mathbf{2}](ClO_4)_2$ in $CDCl_3$ yields 17 partially overlapping signals in the aromatic region [9(L) and 8(bpy)], one CH(acac) proton resonance, and two CH_3(acac) proton resonances corresponding to the half-molecule as expected from the *meso* ($\Delta\Lambda$) diastereomeric form[12] (Figure S2b of the Supporting Information and the Experimental Section).

The identities of $[\mathbf{1}]ClO_4$ and $[\mathbf{2}](ClO_4)_2$ have been authenticated by their single-crystal X-ray structures (Figures 1 and 2). Selected crystallographic and bond parameters are listed in Tables 1 and 2 and Tables S1–S4 of the Supporting Information, respectively.

The structure of mononuclear complex ion $\mathbf{1}^+$ is somewhat similar to that of a reported[5] hexafluoroacetylacetonatopalladium(II) complex with a sterically encumbered Nindigo derivative. There is a five-membered chelate ring of a *cis*-configured Nindigo system (as a protonated dianion) with both indole N coordinated either by the four-coordinate planar Pd^{II}[5] or by the six-coordinate distorted octahedral Ru^{II} (Figure 1). The exocyclic imine N atoms are connected at the opposite side by an asymmetric[5] intramolecular hydrogen bridge [N–H···N angle of 165° and N(H)···N distance of 2.767 Å for $\mathbf{1}^+$]. Some asymmetry is also apparent in the bis-indole

dx.doi.org/10.1021/ic501460d | Inorg. Chem. 2014, 53, 9348–9356

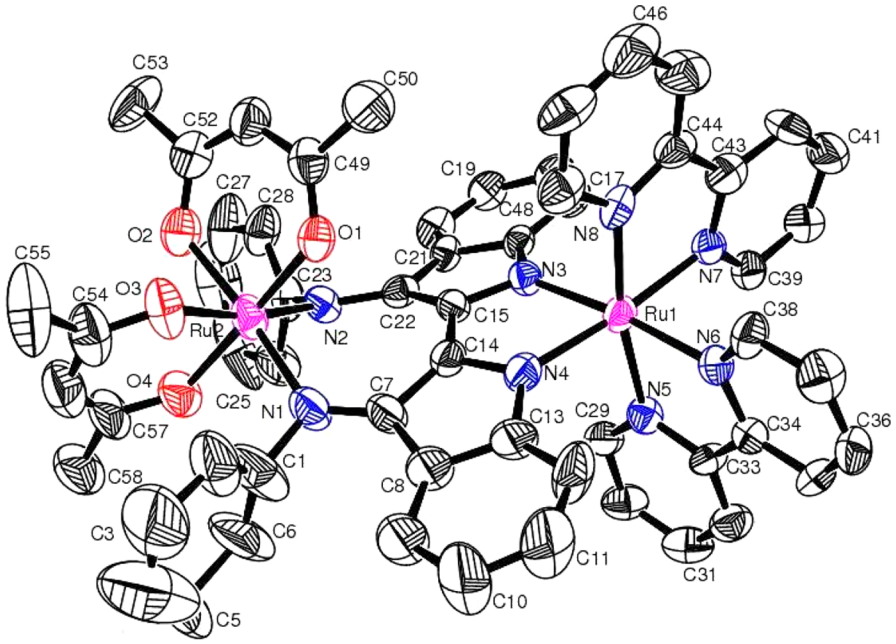

Figure 2. ORTEP diagram of the cationic part of $[2](ClO_4)_2$. Ellipsoids are drawn at the 50% probability level. Hydrogen atoms have been omitted for the sake of clarity.

Table 1. Selected Crystallographic Data for $[1]ClO_4 \cdot C_7H_8$ and $[2](ClO_4)_2$

	$[1]ClO_4 \cdot C_7H_8$	$[2](ClO_4)_2$
empirical formula	$C_{55}H_{43}ClN_8O_4Ru$	$C_{58}H_{48}Cl_2N_8O_{12}Ru_2$
formula weight	1016.49	1322.08
crystal system	triclinic	monoclinic
space group	$P\bar{1}$	$P2_1/c$
a (Å)	12.2450(7)	9.5175(4)
b (Å)	13.6473(6)	25.1198(14)
c (Å)	15.3141(8)	27.4990(11)
α (deg)	99.265(4)	90
β (deg)	110.594(5)	95.044(4)
γ (deg)	90.416(4)	90
V (Å^3)	2358.7(2)	6548.9(5)
Z	2	4
μ (mm^{-1})	0.446	0.603
T (K)	150(2)	150(2)
D_{calcd} (g cm^{-3})	1.431	1.341
$F(000)$	1044	2680
θ range (deg)	2.99–25.00	3.08–25.00
data/restraints/parameters	8297/0/626	11509/0/743
R1, wR2 [$I > 2\sigma(I)$]	0.0451, 0.1036	0.0921, 0.2451
R1, wR2 (all data)	0.0616, 0.1134	0.1485, 0.2818
GOF	1.025	1.016
largest difference peak/hole (e Å^{-3})	0.989/−0.413	0.899/−1.012

framework of LH^-; however, the overall description of the system as $[Ru^{II}(bpy)_2(LH^-)]ClO_4$ is well-supported by the metric parameters.

Attempts to obtain a bis-$[Ru(bpy)_2]^{2+}$ complex of the deprotonated Nindigo molecule were unsuccessful. However, reaction of mononuclear $[1]ClO_4$ with $[Ru(acac)_2(CH_3CN)_2]$ in an EtOH/NEt_3 mixture yielded asymmetric dinuclear[13] complex ion 2^{2+} as bis-perchlorate. Its structure determination, although marred by less satisfactory crystal quality, indicates the $\Delta\Lambda$ configuration for the molecules (cf. ^{1}H NMR) and confirms that the $[Ru(acac)_2]$ moiety in 2^{2+} has been coordinated by chelating exocyclic imine N atoms to form a distinctly nonplanar seven-membered ring, best described by an envelope conformation with the metal (Ru2) sticking out of the conjugated NCCCCN plane (Figure 2 and Figure S3 of the Supporting Information).

Seven-membered chelate rings involving ruthenium were hitherto observed only for saturated systems.[14] The nearly planar five-membered ring chelate involving $[Ru(bpy)_2]$ remains almost unchanged, and there is no significant difference in the steric requirements between $[Ru(bpy)_2]^{2+}$ and $[Ru(acac)_2]^+$ groups. As a result, the dinuclear complex exhibits one metal, Ru1, part of three five-membered chelate rings involving α-diimine functions, whereas the other ruthenium center, Ru2, is surrounded by negatively charged chelate ligands forming a six-membered ($acac^-$) or seven-membered ($Nindigo^-$) ring. Metric parameters of the bridge (Table 2) and the coordination environments suggest the +II oxidation state for the tris(diimine)-coordinated Ru1 (average Ru−N distance of 2.064 Å) and an $acac^-$-stabilized[15] +III state for Ru2 (average Ru−N/Ru−O distance of 2.014 Å), leaving by implication a radical anion formulation for the (twisted) bridge. The overall diamagnetism of 2^{2+} is then attributed to strong antiferromagnetic coupling between Ru^{III} and the Nindigo radical anion. The broken symmetry calculations for 2^{2+} also predict identical energy for the broken symmetry singlet state and the closed shell singlet form. Density functional theory (DFT) calculations (Table 2) confirm the experimental structure and the assignment of oxidation states.

Both the mononuclear (1^+) and dinuclear (2^{2+}) complexes display multiple redox processes within the potential window of ±2 V in CH_3CN versus SCE (Figure 3 and Table 3). The comproportionation constant values for the intermediate redox states [$RT \ln K_c = nF(\Delta E)$, where ΔE is the difference in redox potentials between successive redox processes[16]] vary in the range of 10^3–10^{13} (Table 3). The electrochemical data in Figure 3 (Table 3) reveal that oxidation processes in 1^+ take place at a potential appreciably lower than that of processes in

dx.doi.org/10.1021/ic501460d | Inorg. Chem. 2014, 53, 9348–9356

Table 2. Selected Experimental and Density Functional Theory (DFT)-Calculated Bond Lengths for $[1]ClO_4$ and $[2](ClO_4)_2$

$[1]ClO_4 \cdot C_7H_8$			$[2](ClO_4)_2$		
bond length (Å)	X-ray	DFT	bond length (Å)	X-ray	DFT
Ru(1)−N(3)	2.086(3)	2.125	Ru(1)−N(3)	2.058(6)	2.122
Ru(1)−N(4)	2.071(3)	2.118	Ru(1)−N(4)	2.044(7)	2.120
Ru(1)−N(5)	2.044(3)	2.094	Ru(1)−N(5)	2.079(7)	2.100
Ru(1)−N(6)	2.041(3)	2.111	Ru(1)−N(6)	2.067(7)	2.117
Ru(1)−N(7)	2.041(3)	2.118	Ru(1)−N(7)	2.083(7)	2.124
Ru(1)−N(8)	2.055(3)	2.097	Ru(1)−N(8)	2.051(7)	2.120
N(1)−C(7)	1.363(5)	1.356	Ru(2)−N(1)	2.029(9)	2.061
N(2)−C(22)	1.305(4)	1.296	Ru(2)−N(2)	1.963(7)	2.014
N(3)−C(15)	1.349(4)	1.355	Ru(2)−O(1)	2.000(6)	2.068
N(3)−C(16)	1.402(4)	1.398	Ru(2)−O(2)	2.017(7)	2.054
N(4)−C(13)	1.373(4)	1.367	Ru(2)−O(3)	2.027(7)	2.060
N(4)−C(14)	1.392(4)	1.390	Ru(2)−O(4)	2.051(7)	2.077
C(7)−C(8)	1.420(5)	1.432	N(1)−C(7)	1.296(12)	1.310
C(7)−C(14)	1.417(5)	1.444	N(2)−C(22)	1.365(10)	1.340
C(8)−C(13)	1.436(5)	1.438	N(3)−C(15)	1.339(10)	1.350
C(14)−C(15)	1.411(5)	1.405	N(3)−C(16)	1.395(10)	1.397
C(15)−C(22)	1.468(5)	1.490	N(4)−C(13)	1.438(12)	1.409
C(16)−C(21)	1.409(5)	1.420	N(4)−C(14)	1.385(10)	1.335
C(21)−C(22)	1.475(5)	1.470	C(7)−C(8)	1.450(14)	1.473
N(1)−H	0.92(5)	1.035	C(7)−C(14)	1.453(13)	1.485
N(2)···H(N)	1.872	1.771	C(8)−C(13)	1.421(15)	1.416
N(1)···N(2)	2.767	2.762	C(14)−C(15)	1.418(12)	1.431
			C(15)−C(22)	1.441(10)	1.455
			C(16)−C(21)	1.437(10)	1.422
			C(21)−C(22)	1.461(11)	1.454

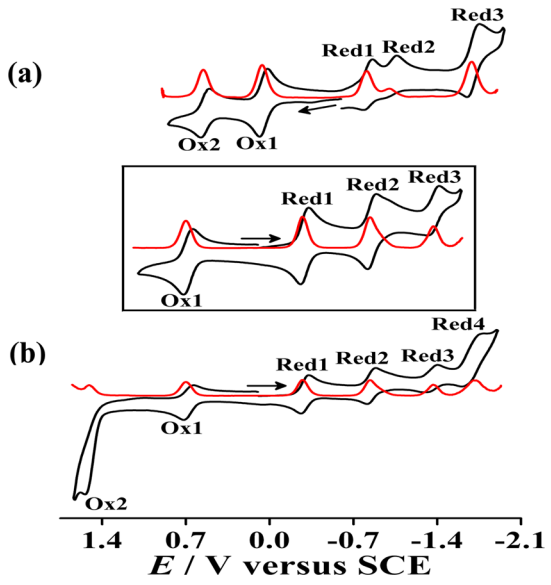

Figure 3. Cyclic (black) and differential pulse (red) voltammograms of (a) $[1]ClO_4$ and (b) $[2](ClO_4)_2$ in CH_3CN. Scan rate of 100 mV/s. The inset shows the segmented part of panel b.

2^{2+} while reduction processes are more facile in 2^{2+}. Spectroelectrochemistry experiments (see later) establish the reversibility of Ox1, Ox2, and Red1 for 1^+ and of Ox1, Red1, and Red2 for 2^{2+} (Figure 3).

Electron paramagnetic resonance (EPR) and ultraviolet−visible−near-infrared (UV−vis−NIR) spectroelectrochemistry[17,18] in conjunction with DFT results (Tables S5−S19 and Figures S4 and S6 of the Supporting Information) have been employed to assign the electrogenerated intermediates and thus identify the electron transfer processes associated with redox series 1^n and 2^n.

X-Band EPR spectra are shown in Figures 4 and 5 and Figure S5 of the Supporting Information; the corresponding data are summarized in Table 4. Pertinent spin densities from DFT calculations for several paramagnetic species are illustrated in Figure 6 and Figure S6 of the Supporting Information and listed in Table 5 and Table S19 of the Supporting Information.

Reduction of compound $[1]ClO_4$ at room temperature inside the EPR cavity[18] produces a slightly resolved solution spectrum with ^{14}N hyperfine coupling at 0.325 and 0.360 mT. The slight discrepancy between the ^{14}N parameters is suggested by the spectral simulation and is attributed to the asymmetric structure. This splitting is assigned to coupling with the coordinating N(indole) nuclei of the redox-active Nindigo ligand that, like the isotropic g factor of 2.0025 and the DFT-calculated spin density (Table 5), confirm a ligand (Nindigo) radical coordinated by ruthenium(II).[18,19] Oxidation of $[1]ClO_4$, possibly proceeding under the loss of H^+,[20] yields an EPR signal (Figure S5 of the Supporting Information) only in the frozen state at 110 K, the notable anisotropy $\Delta g = 0.086$ of the g components suggesting more metal contributions to the singly occupied MO, which is evident from the calculated spin density (Table 5). Compound 1^+ thus exhibits a typical[18] behavior of $[Ru(bpy)_2(L)]$ complexes with partially metal-involving oxidation and mostly ligand-centered reduction.

In contrast, the oxidation and reduction of complex $[2](ClO_4)_2$ yield intermediates with largely metal-centered spin, as confirmed by *in situ* EPR measurements. In agreement with the DFT-calculated spin densities (Table 5), oxidation produces a rather large g anisotropy (Δg) of 0.55 (Figure 5 and Table 4), signifying[19] almost complete localization of the unpaired electron on the metal in 2^{3+}. The somewhat smaller g

dx.doi.org/10.1021/ic501460d | Inorg. Chem. 2014, 53, 9348−9356

Table 3. Electrochemical Data[a] for [1]ClO_4 and [2]$(ClO_4)_2$

	E°_{298} (V) [ΔE (mV)][b]						K_c[c]			
complex	Ox2	Ox1	Red1	Red2	Red3	Red4	K_{c1}[d]	K_{c2}[d]	K_{c3}[d]	K_{c4}[d]
[1]ClO_4	0.54 (80)	0.06 (70)	−0.82 (80)	−1.02 (80)	−1.70 (100)	–	1.4×10^8	2.5×10^3	3.4×10^{11}	–
[2]$(ClO_4)_2$	1.54[e]	0.67 (80)	−0.29 (70)	−0.85 (70)	−1.34 (80)	−1.68 (160)	5.6×10^{13}	3.10×10^9	2.0×10^8	5.8×10^5

[a]From cyclic voltammetry in a CH_3CN/0.1 M Et_4NClO_4 mixture at 100 mV s^{-1}. [b]Potential in volts vs the saturated calomel reference electrode; peak potential differences ΔE_p (in millivolts, in parentheses). [c]Comproportionation constant from $RT \ln K_c = nF(\Delta E)$. [d]$K_{c1}$ between Ox1 and Ox2; K_{c2} between Red1 and Red2; K_{c3} between Red2 and Red3; K_{c4} between Red3 and Red4. [e]Irreversible.

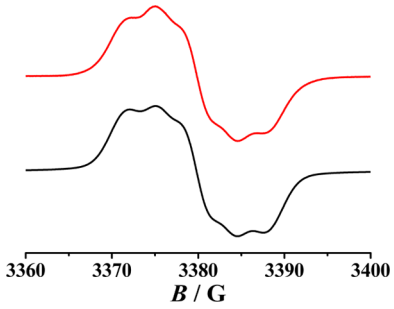

Figure 4. X-Band EPR spectrum of cathodically reduced [1]ClO_4 in a CH_3CN/0.1 M Bu_4NPF_6 mixture at 298 K (black, experimental; red, simulated).

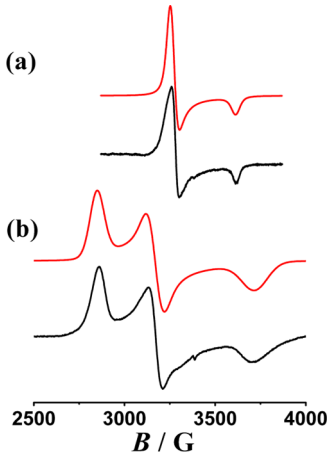

Figure 5. X-Band EPR spectra of electrolytically generated (a) 2^+ (black, experimental; red, simulated) and (b) 2^{3+} (black, experimental; red, simulated) at 110 K in a CH_3N/0.1 M Bu_4NPF_6 mixture.

Table 4. EPR Data[a] from *in Situ* Electrolyses

	1^{2+}	1	2^{3+}	2^+
g_1	2.069	*b*	2.37	2.073
g_2	2.024	*b*	2.13	2.073
g_3	1.983	*b*	1.82	1.873
$\langle g \rangle$[d]	2.025	2.0025[c]	2.12	2.008
Δg[e]	0.086	<0.002[b]	0.55	0.200

[a]In a CH_3CN/0.1 M Bu_4NPF_6 mixture, with measurements at 110 K except for those of **1**. [b]Measurement at 298 K, with no *g* anisotropy observed. [c]Best fit assuming hyperfine splitting from two slightly different ^{14}N nuclei (0.325/0.36 mT). [d]$\langle g \rangle = [{}^1/_3(g_1^2 + g_2^2 + g_3^2)]^{1/2}$. [e]$\Delta g = g_1 - g_3$.

anisotropy (Δg = 0.20) for reduced 2^+ and the nearly axial symmetry ($g_1 \approx g_2$) point to a certain mixing of metal and Nindigo ligand orbitals, well reflected by the spin density calculation results of 0.567 and 0.369, respectively (Figure 6 and Table 5).

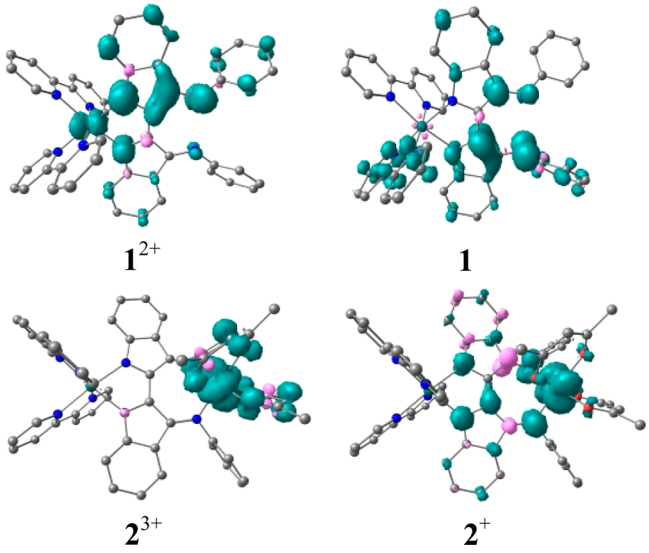

Figure 6. DFT-calculated Mulliken spin density plots of 1^n and 2^n.

Table 5. DFT-Calculated Mulliken Spin Densities for Paramagnetic Forms of 1^n and 2^n

complex	Ru[a]	Ru[b]	acac	bpy	HL/L
1^{2+} ($S = {}^1/_2$)	–	0.125	–	−0.006	0.879
1 ($S = {}^1/_2$)	–	−0.014	–	0.249	0.803
2^{3+} ($S = {}^1/_2$)	0.729	−0.012	0.335	0	−0.027
2^+ ($S = {}^1/_2$)	0.567	0.008	0.044	0.008	0.369

[a]$acac^-$-coordinated ruthenium. [b]bpy-coordinated ruthenium.

While the diamagnetic precursors could thus be identified structurally and the one-electron oxidized and reduced forms were characterized by EPR, the further accessible oxidation states were investigated by use of UV−vis−NIR spectroelectrochemistry (Figure 7 and Table 6).[18] Within this approach, the electronic transitions of all available redox states were determined and assigned by time-dependent DFT (TD-DFT) calculations (Tables 7 and 8) because both the tris(chelate) ruthenium species[10,11] and the indigo/Nindigo π systems[6,21] continue to be extensively investigated chromophores.

Mononuclear 1^+ exhibits a moderately intense, broad near-infrared (NIR) absorption at λ_{max} = 1086 nm that is mainly attributed to a HOMO−LUMO transition of metal-to-ligand charge transfer (MLCT) character. More MLCT absorptions from low-lying occupied MOs occur in the visible region. Upon reduction to neutral Ru^{II}−radical complex **1**, a ligand-to-ligand (Nindigo-to-bipyridine) charge transfer (LLCT) band appears in the NIR region at 973 nm with higher-energy transitions to the π^* MO of LH^- in the visible region. One-electron oxidation to a species with a mixed metal/ligand spin distribution also produces NIR absorptions at λ_{max} = 1103 and 1279 nm that are assigned to transitions directed at the π^* MO of the Nindigo

dx.doi.org/10.1021/ic501460d | Inorg. Chem. 2014, 53, 9348−9356

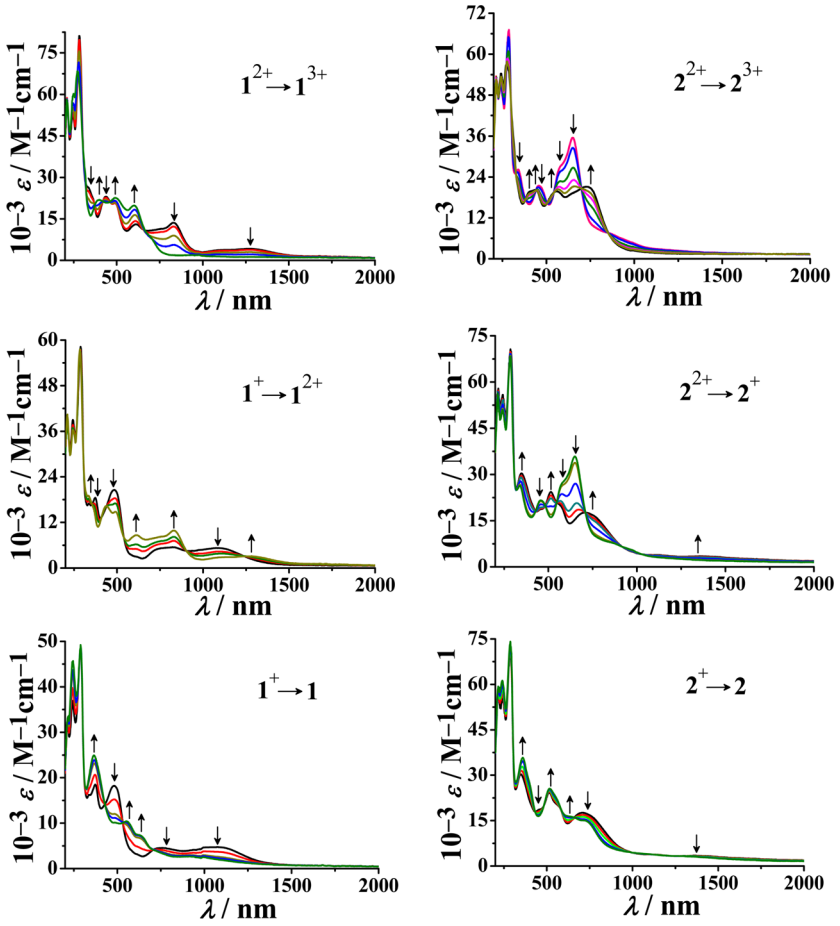

Figure 7. UV−vis−NIR spectroelectrochemistry of $\mathbf{1}^n$ (left) and $\mathbf{2}^n$ (right) in a CH_3CN/0.1 M NBu_4PF_6 mixture.

Table 6. UV−Vis−NIR Spectroelectrochemical Data of $\mathbf{1}^n$ and $\mathbf{2}^n$ in a CH_3CN/0.1 M Bu_4NPF_6 Mixture

complex	λ (nm) [ε (M^{-1} cm^{-1})]
$\mathbf{1}^{3+}$	600 (19860), 493 (22680), 395 (21880)
$\mathbf{1}^{2+}$	1279 (3120), 1103 (2820), 831 (10120), 614 (8660), 490 (14890), 437 (16360), 332 (sh, 19000)
$\mathbf{1}^{+}$	1086 (4730), 738 (4520), 484 (18190), 373 (18500), 337 (16210)
1	973 (2510), 635 (7270), 555 (10420), 365 (24930)
$\mathbf{2}^{3+}$	734 (21160), 557 (19790), 438 (20200), 406 (sh, 19740)
$\mathbf{2}^{2+}$	650 (35810), 575 (sh, 27010), 456 (21670), 339 (26410)
$\mathbf{2}^{+}$	1370 (3450), 1124 (3850), 710 (17650), 569 (sh, 19930), 514 (24370), 349 (30370)
2	725 (15000), 646 (16290), 517 (25580), 360 (35860)

ligand. Similar transitions, albeit at lower wavelengths, occur for the two-electron-oxidized form.

Structurally characterized dinuclear ion $\mathbf{2}^{2+}$ exhibits intense absorptions in the visible region. In agreement with the oxidation state assignment (Scheme 2), the transitions are of mixed character such as MLCT/LLCT. Oxidation to a pure ruthenium(III) species $\mathbf{2}^{3+}$ causes shifts of bands in the visible region. Reduction to $\mathbf{2}^{+}$ with still mostly metal-based spin produces some moderately intense NIR absorptions that are caused by transitions to the π^*(bpy) MO. The second reduction to neutral **2** produces similar transitions; however, these occur at higher energies. The TD-DFT calculations of the $\mathbf{2}^n$ series do not reveal any major features that can be attributed to intervalence charge transfer, in agreement with the class I assignment according to the Robin/Day classification.

CONCLUSION

The purpose of this study is to demonstrate the coordinative options of the noninnocent Nindigo ligand, depending on the ancillary ligands at the redox-active ruthenium centers. In contrast to the recently described successful coordination of two $[Ru(acac)_2]$ entities to *trans*-Nindigo,[4] the use of $[Ru(bpy)_2]^{2+}$ moieties did not result in a Nindigo-bridged dinuclear complex. A 1:1 coordination does take place to yield $\mathbf{1}^{+}$; however, it involves both indole N donors in a five-membered ring chelate situation with the *cis* configuration of the Nindigo ligand and intramolecular hydrogen bonding. The strong preference of $[Ru^{II}(bpy)_2]^{2+}$ for an α-diimine type coordination is held responsible for this isomerization. Remarkably, this mononuclear precursor can add a $[Ru(acac)_2]$ fragment under electron exchange to yield $\mathbf{2}^{2+}$ with one tris(α-diimine)-ruthenium(II) center and one Ru^{III} site surrounded by donating $acac^-$ and a seven-membered ring chelate provided by deprotonated *cis*-Nindigo. Nindigo has thus been recognized for the first time to act as an asymmetric but still highly redox-active ligand bridge as has been demonstrated by experiments (EPR and UV−vis−NIR spectroelectrochemistry) and the results of TD-DFT calculations on corresponding redox series. Studies with other metal complexes will have to clarify which factors favor the *cis* versus *trans* configuration of the noninnocent Nindigo bridging ligands.

EXPERIMENTAL SECTION

Materials. The metal precursors $[Ru^{II}(acac)_2(CH_3CN)_2]$,[22] *cis*-$[Ru^{II}(bpy)_2Cl_2]\cdot 2H_2O$,[23] and the ligand indigo-bis(*N*-phenylimine)[24]

dx.doi.org/10.1021/ic501460d | Inorg. Chem. 2014, 53, 9348−9356

Table 7. TD-DFT (B3LYP/CPCM/CH_3CN)-Calculated Electronic Transitions for 1^n

λ (nm), expt (DFT)	ε (M^{-1} cm^{-1}) (f)	transitions	character
		1^{3+} (S = 0)	
600 (626)	19860 (0.173)	HOMO-3 → LUMO (0.55)	HL(π)/Ru(dπ) → HL(π^*)
		HOMO-4 → LUMO (0.32)	Ru(dπ)/bpy(π) → HL(π^*)
493 (506)	22680 (0.251)	HOMO-9 → LUMO (0.44)	bpy(π)/HL(π) → HL(π^*)
		HOMO-1 → LUMO (0.41)	HL(π)/Ru(dπ) → HL(π^*)
395 (449)	21880 (0.101)	HOMO-3 → LUMO +1 (0.67)	HL(π)/Ru(dπ) → HL(π^*)
		1^{2+} (S = $^1/_2$)	
1279 (1302)	3120 (0.004)	HOMO(β) → LUMO(β) (0.96)	HL(π)/Ru(dπ) → HL(π^*)
1103 (1065)	2820 (0.051)	SOMO(α) → LUMO(α) (0.93)	HL(π) → HL(π^*)
831 (796)	10120 (0.135)	HOMO-1(β) → LUMO(β) (0.90)	HL(π) → HL(π^*)
614 (599)	8660 (0.089)	HOMO(β) → LUMO+1(β) (0.67)	HL(π)/Ru(dπ) → HL(π^*)
		SOMO-1(α) → LUMO(α) (0.46)	HL(π)/Ru(dπ) → HL(π^*)
490 (474)	14890 (0.174)	HOMO(β)-3 → LUMO+1(β) (0.58)	Ru(dπ) → HL(π^*)
437 (438)	16360 (0.103)	SOMO(α) → LUMO +3(α) (0.61)	HL(π) → bpy(π^*)
332 (326)	19000 (0.090)	HOMO(β) → LUMO+5(β) (0.38)	HL(π)/Ru(dπ) → bpy(π^*)
		HOMO(β) → LUMO+8(β) (0.28)	HL(π)/Ru(dπ) → HL(π^*)
		1^+ (S = 0)	
1086 (1006)	4730 (0.126)	HOMO → LUMO (0.70)	HL(π)/Ru(dπ) → bpy(π^*)
		HOMO-1 → LUMO (0.11)	HL(π)/Ru(dπ) → bpy(π^*)
738 (700)	4520 (0.058)	HOMO-1 → LUMO (0.69)	HL(π)/Ru(dπ) → bpy(π^*)
484 (489)	18190 (0.235)	HOMO-4 → LUMO (0.54)	HL(π)/Ru(dπ) → bpy(π^*)
		HOMO-3 → LUMO (0.38)	Ru(dπ)/HL(π) → bpy(π^*)
373 (434)	18500 (0.221)	HOMO → LUMO+7 (0.61)	HL(π) → HL(π^*)
		HOMO → LUMO+5 (0.25)	HL(π) → bpy(π^*)
337 (348)	16210(0.105)	HOMO-1 → LUMO +7 (0.51)	HL(π)/Ru(dπ) → HL(π^*)
		HOMO-1 → LUMO +5 (0.21)	HL(π)/Ru(dπ) → bpy(π^*)
		1 (S = $^1/_2$)	
973 (1007)	2510 (0.033)	HOMO(β) → LUMO(β) (0.85)	HL(π) → bpy(π^*)
635 (587)	7270 (0.127)	SOMO(α) → LUMO +6(α) (0.81)	bpy(π)/HL(π) → HL(π^*)
555 (545)	10420 (0.146)	HOMO-2(β) → LUMO+2(β) (0.84)	Ru(dπ)/HL(π) → HL(π^*)
365 (338)	24930 (0.124)	SOMO(α)-8 → LUMO(α) (0.37)	HL(π) → bpy(π^*)/ HL(π^*)

were prepared according to literature procedures. All other chemicals and reagents were of reagent grade and were used without further purification. For spectroscopic and electrochemical studies, high-performance liquid chromatography grade solvents were used.

Physical Measurements. UV−vis−NIR spectroelectrochemical studies were performed in a CH_3CN/0.1 M Bu_4NPF_6 mixture at 298 K, using an optically transparent thin layer electrochemical (OTTLE) cell[25] that was mounted in the sample compartment of a J&M TIDAS spectrophotometer. Fourier transform infrared spectra were recorded on a Nicolet spectrophotometer with samples prepared as KBr pellets. ^1H NMR spectra were recorded on a Bruker Avance III 500 spectrometer. The EPR measurements were taken in a two-electrode capillary tube[18] with an X-band Bruker system (ESP300), equipped with a Bruker ER035M gaussmeter and an HP 5350B microwave counter. Cyclic voltammetric, differential pulse voltammetric, and coulometric measurements were taken using a PAR model 273A electrochemistry system. Platinum wire working and auxiliary electrodes and an aqueous saturated calomel reference electrode (SCE) were used in a three-electrode configuration. The supporting electrolyte was $[Et_4N][ClO_4]$, and the solute concentration was ~10^{-3} M. The half-wave potential, E°_{298}, was set equal to $0.5(E_{pa} + E_{pc})$, where E_{pa} and E_{pc} are anodic and cathodic cyclic voltammetric peak potentials, respectively. The electrical conductivity of the solution was checked by using an Autoranging conductivity meter (Toshcon Industries). The elemental analyses were conducted on a Thermoquest (EA 1112) micro analyzer. Electrospray mass spectra were recorded on a Bruker Microflex matrix-assisted laser desorption ionization time-of-flight (YA-105) mass spectrometer.

Scheme 2. Oxidation State Assignments within Redox Series 1^n and 2^n

$\mathbf{1}^{3+}$-H^+ $[(bpy)_2Ru^{III}(L^{\bullet-})]^{2+}$ ⟷ $[(bpy)_2Ru^{IV}(L^{2-})]^{2+}$

$-e^-$ ⇅ $+e^-$

$\mathbf{1}^{2+}$-H^+ $[(bpy)_2Ru^{III}(L^{2-})]^{+}$ ⟷ $[(bpy)_2Ru^{II}(L^{\bullet-})]^{+}$

$-H^+, -e^-$ ⇅ $+e^-, +H^+$

$\mathbf{1}^{+}$ $[(bpy)_2Ru^{II}(HL^{-})]^{+}$

$-e^-$ ⇅ $+e^-$

$\mathbf{1}^{0}$ $[(bpy)_2Ru^{II}(HL^{\bullet 2-})]^{0}$

$\mathbf{2}^{3+}$ $[(acac)_2Ru^{III}(\mu\text{-}L^{0})Ru^{II}(bpy)_2]^{3+}$

$-e^-$ ⇅ $+e^-$

$\mathbf{2}^{2+}$ $[(acac)_2Ru^{III}(\mu\text{-}L^{\bullet-})Ru^{II}(bpy)_2]^{2+}$

$-e^-$ ⇅ $+e^-$

$\mathbf{2}^{+}$ $[(acac)_2Ru^{III}(\mu\text{-}L^{2-})Ru^{II}(bpy)_2]^{+}$

$-e^-$ ⇅ $+e^-$

$\mathbf{2}^{0}$ $[(acac)_2Ru^{II}(\mu\text{-}L^{2-})Ru^{II}(bpy)_2]^{0}$

Preparation of Complexes. *[(bpy)$_2$Ru(HL)]ClO_4, [1]ClO_4.* A mixture of 100 mg (0.2 mmol) of *cis*-$[Ru(bpy)_2Cl_2]\cdot 2H_2O$ and 83 mg (0.4 mmol) of $AgClO_4$ in 30 mL of absolute ethanol was refluxed under a dinitrogen atmosphere for 2 h. The precipitated AgCl was filtered through a sintered glass funnel. To the filtrate containing $[Ru(bpy)_2(EtOH)_2](ClO_4)_2$ were added 82 mg (0.2 mmol) of H_2L and 21 mg (0.2 mmol) of NEt_3 (freshly distilled over KOH), and the mixture was refluxed under a dinitrogen atmosphere for 14 h. The reaction mixture was evaporated to dryness under reduced pressure. The crude product was purified by using a neutral alumina column. The pure brown complex corresponding to $[\mathbf{1}]ClO_4$ was eluted with a 4:1 dichloromethane/acetonitrile mixture. Evaporation of the solvent

dx.doi.org/10.1021/ic501460d | Inorg. Chem. 2014, 53, 9348−9356

Table 8. TD-DFT (B3LYP/CPCM/CH_3CN)-Calculated Electronic Transitions for 2^n

λ (nm), expt (DFT)	ε (M^{-1} cm^{-1}) (f)	transitions	character
		2^{3+} (S = $^1/_2$)	
734 (689)	21160 (0.188)	SOMO-2(α) → LUMO(α) (0.49)	acac(π)/L(π)/Ru2(dπ) → L(π^*)
		HOMO-6(β) → LUMO(β) (0.34)	L(π)/acac(π)/Ru2(dπ) → L(π^*)/Ru2(dπ)/acac(π^*)
557 (602)	19790 (0.088)	HOMO-7(β) → LUMO(β) (0.34)	L(π)/Ru2(dπ)/acac(π) → L(π^*)/Ru2(dπ)/acac(π^*)
438 (461)	20200 (0.100)	SOMO-4(α) → LUMO+1(α) (0.58)	L(π) → L(π^*)
		HOMO-16(β) → LUMO(β) (0.33)	L(π) → L(π^*)/Ru2(dπ)/acac(π^*)
406 (422)	19740 (0.058)	HOMO-12(β) → LUMO+1(β) (0.53)	bpy(π) → L(π^*)/Ru2(dπ)
		2^{2+} (S = 0)	
650 (618)	35810 (0.298)	HOMO-2 → LUMO+1 (0.40)	Ru2(dπ)/L(π)/acac(π) → bpy(π^*)
575 (599)	27010 (0.049)	HOMO-5 → LUMO (0.65)	L(π)/acac(π) → L(π^*)/Ru2(dπ)
456 (477)	21670 (0.135)	HOMO-6 → LUMO+1 (0.46)	acac(π)/L(π)/Ru1(dπ) → bpy(π^*)
339 (356)	26410 (0.037)	HOMO-14 → LUMO+1 (0.53)	bpy(π) → bpy(π^*)
		2^{+} (S = $^1/_2$)	
1370 (1243)	3450 (0.012)	HOMO-3(β) → LUMO(β) (0.58)	L(π)/Ru1(dπ) → bpy(π^*)
		HOMO-1(β) → LUMO(β) (0.45)	Ru2(dπ)/acac(π)/L(π) → bpy(π^*)
1124 (1070)	3850 (0.032)	HOMO(β) → LUMO(β) (0.64)	L(π)/Ru2(dπ)/acac(π) → bpy(π^*)
710 (683)	17650 (0.103)	SOMO-3(α) → LUMO(α) (0.53)	Ru2(dπ)/L(π) → bpy(π^*)
		SOMO-4(α) → LUMO(α) (0.53)	L(π)/Ru1(dπ) → bpy(π^*)
569 (639)	19930 (0.081)	SOMO-4(α) → LUMO(α) (0.53)	L(π)/Ru1(dπ) → bpy(π^*)
514 (482)	24370 (0.047)	SOMO-7(α) → LUMO(α) (0.53)	Ru1(dπ) → bpy(π^*)
		SOMO-6(α) → LUMO(α) (0.34)	L(π)/acac(π) → bpy(π^*)
349 (328)	30370 (0.081)	SOMO(α) → LUMO+10(α) (0.27)	L(π) → acac(π^*)
		HOMO-2(β) → LUMO+8(β) (0.24)	Ru2(dπ)/acac(π) → L(π^*)/acac(π^*)
		2 (S = 1)	
725 (692)	15000 (0.099)	HOMO-1(β) → LUMO(β) (0.56)	Ru2(dπ)/acac(π) → bpy(π^*)
		HOMO-3(β) → LUMO(β) (0.56)	L(π)/Ru1(dπ) → bpy(π^*)
646 (664)	16290 (0.031)	HOMO-3(β) → LUMO(β) (0.68)	L(π)/Ru1(dπ) → bpy(π^*)
517 (528)	25580 (0.080)	HOMO-4(β) → LUMO(β) (0.61)	L(π)/acac(π)/Ru1(π) → bpy(π^*)
		SOMO1(α) → LUMO+7(α) (0.35)	L(π)/bpy(π) → bpy(π^*)
		SOMO1(α) → LUMO+8(α) (0.35)	L(π)/bpy(π) → acac(π^*)
360 (362)	35860 (0.036)	HOMO-11(β) → LUMO(β) (0.55)	L(π) → bpy(π^*)

under reduced pressure yielded the pure complex [**1**]ClO_4. Yield: 60% (107 mg). ^{1}H NMR in $(CD_3)_2SO$ (J values in hertz): δ 11.50 (s, 1H, NH), 8.79 (d, 8.15, 2H), 8.74 (d, 8.15, 2H), 8.14 (t, 7.85, 7.95, 2H), 8.09 (d, 5.35, 2H), 8.04 (t, 7.9, 7.65, 2H), 7.86 (d, 5.4, 2H), 7.56 (t, 6.45, 6.5, 2H), 7.52 (t, 6.55, 6.40, 2H), 7.39 (t, 7.65, 7.55, 4H), 7.19 (d, 7.45, 4H), 7.15 (t, 7.15, 6.95, 2H), 6.86 (d, 7.75, 2H), 6.74 (t, 7.55, 7.70, 2H), 6.55 (b, 2H), 5.20 (b, 2H). MS (ESI+, MeCN): {[[**1**]ClO_4−ClO_4]$^+$} calcd, m/z 825.20; found, m/z 825.20. IR (KBr) ν (ClO_4^-): 1091, 622 cm^{-1}. Molar conductivity (MeCN): Λ_M = 90 Ω^{-1} cm^2 M^{-1}. Elemental analysis calcd (%) for $C_{48}H_{35}ClN_8O_4Ru$: C, 62.37; H, 3.82; N, 12.12. Found: C, 62.06; H, 3.80; N, 12.32.

*[(acac)$_2$Ru(L)Ru(bpy)$_2$](ClO$_4$)$_2$, [**2**](ClO$_4$)$_2$.* Fifty milligrams (0.05 mmol) of [**1**]ClO_4, 19 mg (0.05 mmol) of Ru(acac)$_2$(CH_3CN)$_2$, and 6 mg (0.05 mmol) of NEt_3 (freshly distilled over KOH) were taken in 20 mL of absolute ethanol, and the mixture was heated to reflux under a dinitrogen atmosphere for 20 h. The solution was concentrated to 5 mL, and a saturated aqueous solution of sodium perchlorate (10 mL) was added. The resulting dark precipitate was filtered and washed with ice-cold water and dried under vacuum. The crude product was purified by column chromatography using a neutral alumina column. The desired blue solution of [**2**]$(ClO_4)_2$ was eluted with a 2:1 dichloromethane/acetonitrile mixture. Evaporation of the solvent under reduced pressure gave pure [**2**]$(ClO_4)_2$. Yield: 80% (57 mg). ^{1}H NMR in $CDCl_3$ (J values in hertz): δ 8.66 (m, 2H), 8.17 (t, 7.80, 7.75, 1H), 8.07 (m, 2H), 7.66 (d, 5.35, 1H), 7.55 (m, 2H), 7.42 (t, 7.80, 7.55, 1H), 7.34 (t, 7.35, 6.2, 1H), 7.25 (d, 8.65, 1H), 7.22 (d, 7.85, 1H), 7.05 (m, 1H), 6.95 (m, 1H), 6.53 (d, 7.80, 1H), 5.80 (m, 2H), 5.04 [s, 1H, CH(acac)], 2.11 [s, 3H, CH_3(acac)], 1.47 [s, 3H, CH_3(acac)]. MS (ESI+, MeCN): {[[**2**]$(ClO_4)_2$-ClO_4]$^+$} calcd, m/z 1223.13; found, m/z 1223.08. IR (KBr) ν (ClO_4^-): 1089, 621 cm^{-1}. Molar conductivity (MeCN): Λ_M = 190 Ω^{-1} cm^2 M^{-1}. Elemental analysis calcd (%) for $C_{58}H_{48}Cl_2N_8O_{12}Ru_2$: C, 52.69; H, 3.66; N, 8.48. Found: C, 52.50; H, 3.56; N, 8.30.

Crystallography. Single crystals of [**1**]ClO_4 and [**2**]$(ClO_4)_2$ were grown by slow evaporation of their 2:1 dichloromethane/toluene and 1:1 dichloromethane/n-hexane solutions, respectively. X-ray crystal data were collected on a CCD Agilent Technologies (Oxford Diffraction) SUPER NOVA diffractometer. Data collection was evaluated by using CrysAlisPro CCD. The data were collected by the standard ϕ−ω scan techniques and scaled and reduced using CrysAlisPro RED. The structures were determined by direct methods using SHELXS-97 and refined by full matrix least squares with SHELXL-97, refining on F^2.[26] All non-hydrogen atoms were refined anisotropically. The remaining hydrogen atoms were placed in geometrically constrained positions and refined with isotropic temperature factors, generally 1.2U_{eq} of their parent atoms. Hydrogen atoms were included in the refinement process as per the riding model.

Computational Details. Full geometry optimizations were conducted by using the DFT method at the (R)B3LYP level for **1**$^+$, **1**$^{3+}$, and **2**$^{2+}$ and at the (U)B3LYP level for **1**$^{2+}$, **1**, **1**$^-$, **1**$^{2-}$, **2**$^{4+}$, **2**$^{3+}$, **2**$^+$, **2**, **2**$^-$, and **2**$^{2-}$.[27] Except for ruthenium, all other elements were assigned the 6-31G* basis set. The LANL2DZ basis set with an effective core potential was employed for the ruthenium atom.[28] The vibrational frequency calculations were performed to ensure that the optimized geometries represent the local minima and there are only positive eigenvalues. All calculations were performed with Gaussian09.[29] Vertical electronic excitations based on (R)B3LYP/(U)-B3LYP-optimized geometries were computed for **1**^{n} (n = 3+, 2+, +, 0, −, or 2−) and **2**^{n} (n = 4+, 3+, 2+, +, 0, −, or 2−) using the time-dependent density functional theory (TD-DFT) formalism[30] in acetonitrile using the conductor-like polarizable continuum model (CPCM).[31] Chemissian version 1.7[32] was used to calculate the

dx.doi.org/10.1021/ic501460d | Inorg. Chem. 2014, 53, 9348−9356

fractional contributions of various groups to each molecular orbital. All calculated structures were visualized with ChemCraft.[33]

■ ASSOCIATED CONTENT

Supporting Information

X-ray crystallographic files in CIF format for $[\mathbf{1}]ClO_4$ and $[\mathbf{2}](ClO_4)_2$, mass spectra (Figure S1), ^1H NMR data (Figure S2), conformation of $\mathbf{2}^{2+}$ (Figure S3), EPR of $\mathbf{1}^{2+}$ (Figure S5), crystal data (Tables S1−S4), DFT data set for $\mathbf{1}^n$ and $\mathbf{2}^n$ (Tables S1−S19 and Figures S4 and S6). This material is available free of charge via the Internet at http://pubs.acs.org. CCDC: 1009182 ($[\mathbf{1}]ClO_4$), 1009183 $[[\mathbf{2}](ClO_4)_2]$ contain supplementary crystallographic data for this paper. These data can be obtained free of charge from The Cambridge Crystallographic Data center via www.ccdc.cam.ac.uk/data_request/cis.

■ AUTHOR INFORMATION

Corresponding Authors

*E-mail: lahiri@chem.iitb.ac.in.

*E-mail: kaim@iac.uni-stuttgart.de.

Notes

The authors declare no competing financial interest.

■ ACKNOWLEDGMENTS

Financial support received from the Department of Science and Technology, Council of Scientific and Industrial Research (fellowship to P.M.), and the University Grants Commission (fellowship to R.R.), New Delhi (India), the DAAD, FCI, and DFG (Germany) is gratefully acknowledged.

■ REFERENCES

(1) Kaim, W. *Inorg. Chem.* **2011**, *50*, 9752.

(2) (a) Kaim, W.; Lahiri, G. K. *Angew. Chem.* **2007**, *119*, 1808. (b) *Angew. Chem., Int. Ed.* **2007**, *46*, 1778. (c) Kaim, W.; Sarkar, B. *Coord. Chem. Rev.* **2007**, *251*, 584.

(3) (a) Ernst, S.; Hänel, P.; Jordanov, J.; Kaim, W.; Kasack, V.; Roth, E. *J. Am. Chem. Soc.* **1989**, *111*, 1733. (b) Roy, S.; Sarkar, B.; Imrich, H.-G.; Fiedler, J.; Záliš, S.; Jiménez -Aparicio, R.; Urbanos, F. A.; Mobin, S. M.; Lahiri, G. K.; Kaim, W. *Inorg. Chem.* **2012**, *51*, 9273.

(4) Mondal, P.; Ehret, F.; Bubrin, M.; Das, A.; Mobin, S. M.; Kaim, W.; Lahiri, G. K. *Inorg. Chem.* **2013**, *52*, 8467.

(5) Nawn, G.; Waldie, K. M.; Oakley, S. R.; Peters, B. D.; Mandel, D.; Patrick, B. O.; McDonald, R.; Hicks, R. G. *Inorg. Chem.* **2011**, *50*, 9826.

(6) Newn, G.; Oakley, S. R.; Majewski, M. B.; McDonald, R.; Patrick, B. O.; Hicks, R. G. *Chem. Sci.* **2013**, *4*, 612.

(7) Nawn, G.; McDonald, R.; Hicks, R. G. *Inorg. Chem.* **2013**, *52*, 10912.

(8) Fortier, S.; González-del Moral, O.; Chen, C.-H.; Pink, M.; Le Roy, J. J.; Murugesu, M.; Mindiola, D. J.; Caulton, K. G. *Chem. Commun.* **2012**, *48*, 11082.

(9) Fortier, S.; Le Roy, J. J.; Chen, C.-H.; Vieru, V.; Murugesu, M.; Chibotaru, L. F.; Mindiola, D. J.; Caulton, K. G. *J. Am. Chem. Soc.* **2013**, *135*, 14670.

(10) Juris, A.; Balzani, V.; Barigelletti, F.; Campagna, S.; Belser, P.; von Zelewsky, A. *Coord. Chem. Rev.* **1988**, *84*, 85.

(11) Kalyanasundaram, K.; Grätzel, M. *Coord. Chem. Rev.* **1998**, *77*, 347.

(12) (a) Maji, S.; Sarkar, B.; Mobin, S. M.; Fiedler, J.; Urbanos, F. A.; Jiménez-Aparicio, R.; Kaim, W.; Lahiri, G. K. *Inorg. Chem.* **2008**, *47*, 5204. (b) Kumbhakar, D.; Sarkar, B.; Maji, S.; Mobin, S. M.; Fiedler, J.; Urbanos, F. A.; Jiménez-Aparicio, R.; Kaim, W.; Lahiri, G. K. *J. Am. Chem. Soc.* **2008**, *130*, 17575.

(13) Das, A.; Scherer, T. M.; Chowdhury, A. D.; Mobin, S. M.; Kaim, W.; Lahiri, G. K. *Inorg. Chem.* **2012**, *51*, 1675.

(14) (a) Pal, S.; Pal, S. *Polyhedron* **2003**, *22*, 867. (b) Chiu, W.-H.; Guo, C.-X.; Cheung, K.-K.; Che, C.-M. *Inorg. Chem.* **1996**, *35*, 540. (c) Grasa, G. A.; Zanotti-Gerosa, A.; Medlock, J. A.; Hems, W. P. *Org. Lett.* **2005**, *7*, 1449. (d) Arai, N.; Akashi, M.; Sugizaki, S.; Ooka, H.; Inoue, T.; Ohkuma, T. *Org. Lett.* **2010**, *12*, 3380.

(15) Das, D.; Das, A. K.; Sarkar, B.; Mondal, T. K.; Mobin, S. M.; Fiedler, J.; Záliš, S.; Urbanos, F. A.; Jiménez-Aparicio, R.; Kaim, W.; Lahiri, G. K. *Inorg. Chem.* **2009**, *48*, 11853.

(16) Creutz, C. *Prog. Inorg. Chem.* **1983**, *30*, 1.

(17) Kaim, W.; Fiedler, J. *Chem. Soc. Rev.* **2009**, *38*, 3373.

(18) Kaim, W.; Ernst, S.; Kasack, V. *J. Am. Chem. Soc.* **1990**, *112*, 173.

(19) Patra, S.; Sarkar, B.; Mobin, S. M.; Kaim, W.; Lahiri, G. K. *Inorg. Chem.* **2003**, *42*, 6469.

(20) DFT calculations for species in the gas phase show a lower energy for $[(bpy)_2Ru(L\text{-}H)]^{2+}$ than for $[(bpy)_2Ru(L)]^{+}$. However, the deprotonation may be more favorable in an electrolyte-containing solution, the pK_a typically decreasing strongly upon oxidation.

(21) (a) Zollinger, H. *Color Chemistry. Syntheses, Properties and Applications of Organic Dyes and Pigments*, 2nd ed.; VCH: Weinheim, Germany, 1991. (b) Serrano-Andrés, L.; Roos, B. O. *Chem.—Eur. J.* **1997**, *3*, 717. (c) Steingruber, E. Indigo and Indigo Colorants. In *Ullmann's Encyclopedia of Industrial Chemistry*; Wiley-VCH: Weinheim, Germany, 2004; p 1.

(22) Kobayashi, T.; Nishina, Y.; Shinizu, K. G.; Satô, G. P. *Chem. Lett.* **1988**, 1137.

(23) Sullivan, B. P.; Salmon, D. J.; Meyer, T. J. *Inorg. Chem.* **1978**, *17*, 3334.

(24) Oakley, S. R.; Nawn, G.; Waldie, K. M.; Maclnnis, T. D.; Patrick, B. O.; Hicks, R. G. *Chem. Commun.* **2010**, *46*, 6753.

(25) Krejcik, M.; Danek, M.; Hartl, F. *J. Electroanal. Chem.* **1991**, *317*, 179.

(26) (a) Sheldrick, G. M. *Acta Crystallogr., Sect. A* **2008**, *A64*, 112. (b) *Program for Crystal Structure Solution and Refinement*; University of Göttingen: Göttingen, Germany, 1997.

(27) Lee, C.; Yang, W.; Parr, R. G. *Phys. Rev. B* **1988**, *37*, 785.

(28) (a) Andrae, D.; Haeussermann, U.; Dolg, M.; Stoll, H.; Preuss, H. *Theor. Chim. Acta* **1990**, *77*, 123. (b) Fuentealba, P.; Preuss, H.; Stoll, H.; Szentpaly, L. V. *Chem. Phys. Lett.* **1989**, *89*, 418.

(29) Frisch, M. J.; Trucks, G. W.; Schlegel, H. B.; Scuseria, G. E.; Robb, M. A.; Cheeseman, J. R.; Scalmani, G.; Barone, V.; Mennucci, B.; Petersson, G. A.; Nakatsuji, H.; Caricato, M.; Li, X.; Hratchian, H. P.; Izmaylov, A. F.; Bloino, J.; Zheng, G.; Sonnenberg, J. L.; Hada, M.; Ehara, M.; Toyota, K.; Fukuda, R.; Hasegawa, J.; Ishida, M.; Nakajima, T.; Honda, Y.; Kitao, O.; Nakai, H.; Vreven, T.; Montgomery, J. A., Jr.; Peralta, J. E.; Ogliaro, F.; Bearpark, M.; Heyd, J. J.; Brothers, E.; Kudin, K. N.; Staroverov, V. N.; Kobayashi, R.; Normand, J.; Raghavachari, K.; Rendell, A.; Burant, J. C.; Iyengar, S. S.; Tomasi, J.; Cossi, M.; Rega, N.; Millam, J. M.; Klene, M.; Knox, J. E.; Cross, J. B.; Bakken, V.; Adamo, C.; Jaramillo, J.; Gomperts, R.; Stratmann, R. E.; Yazyev, O.; Austin, A. J.; Cammi, R.; Pomelli, C.; Ochterski, J. W.; Martin, R. L.; Morokuma, K.; Zakrzewski, V. G.; Voth, G. A.; Salvador, P.; Dannenberg, J. J.; Dapprich, S.; Daniels, A. D.; Farkas, O.; Foresman, J. B.; Ortiz, J. V.; Cioslowski, J.; Fox, D. J. *Gaussian 09*, revision A.02; Gaussian, Inc.: Wallingford, CT, 2009.

(30) (a) Bauernschmitt, R.; Ahlrichs, R. *Chem. Phys. Lett.* **1996**, *256*, 454. (b) Stratmann, R. E.; Scuseria, G. E.; Frisch, M. J. *J. Chem. Phys.* **1998**, *109*, 8218. (c) Casida, M. E.; Jamorski, C.; Casida, K. C.; Salahub, D. R. *J. Chem. Phys.* **1998**, *108*, 4439.

(31) (a) Barone, V.; Cossi, M. *J. Phys. Chem. A* **1998**, *102*, 1995. (b) Cossi, M.; Barone, V. *J. Chem. Phys.* **2001**, *115*, 4708. (c) Cossi, M.; Rega, N.; Scalmani, G.; Barone, V. *J. Comput. Chem.* **2003**, *24*, 669.

(32) O'Boyle, N. M.; Tenderholt, A. L.; Langner, K. M. *J. Comput. Chem.* **2008**, *29*, 839.

(33) Zhurko, D. A.; Zhurko, G. A. *ChemCraft 1.5*; Plimus: San Diego (available at http://www.chemcraftprog.com).